Journal of the European Ceramic Society 38 (2018) 1888–1896

Contents lists available at ScienceDirect

Journal of the European Ceramic Society

journal homepage: www.elsevier.com/locate/jeurceramsoc

Full Length Article

Gradient thermal cyclic behaviour of $La_2Zr_2O_7$/YSZ DCL-TBCs with equivalent thermal insulation performance

Bo Cheng, Guan-Jun Yang*, Qiang Zhang, Ning Yang, Meng Zhang, Yuming Zhang, Cheng-Xin Li, Chang-Jiu Li

State Key Laboratory for Mechanical Behavior of Materials, School of Materials Science and Engineering, Xi'an Jiaotong University, Xi'an, Shaanxi Province, 710049, PR China

ARTICLE INFO

Keywords:
Thermal barrier coatings
Double ceramic layer
Equivalent thermal insulation
Thermal cyclic lifetime
Failure

ABSTRACT

Thermal insulation performance is a measure of the thermal protection function offered by the thermal barrier coatings (TBCs) to the substrate. In this study, a series of $La_2Zr_2O_7$ (LZO)/YSZ DCL-TBCs, with the equivalent thermal insulation to 500 μm thick YSZ TBCs were prepared, and their lifetimes were evaluated by thermal gradient cyclic test at the top coat surface temperature of 1300 °C. Results show that, the lifetime of DCL-TBCs was more than doubled compared to 500 μm thick YSZ TBCs, when 100 μm and 200 μm thick YSZ coating was substituted by LZO coating. With the increase of LZO substitutional ratio, the delamination position transferred from near top/bond coating interface to near the LZO/YSZ interface and finally to the inside of the LZO coating. The porosity and elastic modulus present a differential distribution across the thickness of top coat. This study provides some data for the composite structure design of next generation advanced DCL-TBCs.

1. Introduction

Elevated operating temperature is beneficial for improving efficiency and performance of both air engine and land-based gas turbines. Thermally sprayed thermal barrier coatings (TBCs) have been used successfully in hot section components to protect the metal parts from hot gases, enabling modern gas-turbine engines to operate at gas temperatures well above the melting temperature of the superalloy [1,2]. The typical TBC is composed of a superalloy substrate, a MCrAlY (M = Ni, Co, NiCo or CoNi) bond coat (BC) to relieve the thermal mismatch between the ceramic layer and the substrate, a thermally grown oxide (TGO) inevitably grown on bond coat surface, and the outermost layer as the top ceramic coats to provide thermal insulation effect [3,4]. The state-of-the-art top coat TBC material is 7–8 wt.% yttria-stabilized zirconia (8YSZ), primarily due to its high toughness and high coefficient of thermal expansion (CTE), and relatively low thermal conductivity [5,6]. However, during long time exposure to high temperature, the most critical issue for YSZ is the limited operation temperature (< 1200 °C) for long-term application. At higher temperature, YSZ may experience phase transformations from non-equilibrium tetragonal (t') phase to tetragonal (t) and cubic (c) phases, and the t-phase further to monoclinic (m) phase during cooling, accompanying volume change [7–9]; Furthermore, higher temperature induces the sintering of ceramic top coating (leading to the reduction of strain tolerance and porosity in combination with the increase of elastic modulus and thermal conductivity), which eventually would accelerate the failure of TBCs [10–12]. The next-generation advanced gas engines require higher turbine inlet temperature (i.e > 1250 °C) [13,14], which means higher surface temperature on TBC surface, and the conventional YSZ can not be competent to endure the harsher operating conditions.

To overcome the shortcomings of YSZ and develop the higher temperature TBCs, pyrochlore structured oxides $La_2Zr_2O_7$ (LZO) are intensively reported since the early study of LZO as the advanced top coat material by R. Vassen et al. [15] reported the double-layer TBCs based on pyrochlore/YSZ in 2004. LZO is phase-stable up to melting points (2300 °C) [3]. What's more, $La_2Zr_2O_7$ shows lower thermal conductivity [16], and the low diffusivity of oxygen ions in $La_2Zr_2O_7$ might decelerates the growth of TGO [17]. However, $La_2Zr_2O_7$ exhibits a low CTE and a poor fracture toughness, which may cause premature failure of the coating during service [16,18]. Given this, LZO/YSZ coatings have been study extensively investigated [13,19–22] to prolong the lifetime of the pyrochlore structured TBCs.

For double ceramic layer TBCs, the new TBC material is prepared on up layer to protect YSZ from higher temperature, and at the same time, the under layer YSZ alleviates the stress between up layer and the substrate. H. Dai et al. [13] reported that, the lifetime of LZO/YSZ DCL TBCs (300 μm top coat, gradient thermal cyclic test) changed with the LZO/YSZ thickness ratio, from several to about 950 cycles

* Corresponding author.
E-mail address: ygj@mail.xjtu.edu.cn (G.-J. Yang).

http://dx.doi.org/10.1016/j.jeurceramsoc.2017.10.058
Received 16 April 2017; Received in revised form 26 October 2017; Accepted 29 October 2017
Available online 04 November 2017

(1250 ± 30 °C), and the lifetime of LZO/YSZ TBCs can be beyond the pure YSZ coating.

L. Wang et al. [21] reported the thermal shock behavior of DCL-TBCs composed of pure YSZ and nanostructured YSZ, and the lifetime of DCL-TBC could be longer than that of conventional single ceramic layer TBCs. Hence, the DCL-TBCs architecture could be an effective development direction to satisfy the requirements of higher temperature applications, since no single material that has been reported so far satisfies all requirements for high temperature TBCs.

However, thermal insulation effect, as one of the fundamental functions, should be paid preferential attention. It is a measure of the thermal protection offered by the TBC to the substrate. In the reported literature, the design of DCL coatings is based on same total thickness of top coating while the thickness ratio of LZO to YSZ is changed. Since the thermal conductivity of LZO is much lower than that of YSZ, the thermal insulation effect of DCL coatings and the pure YSZ is evidently different from one to another. A theoretical basis must be established for the design of DCL TBCs towards a fair and comprehensive understanding of their thermal cyclic behavior.

In this paper, based on the theoretical basis of same thermal barrier effect, a series of LZO/YSZ TBCs were designed and prepared for the gradient thermal cyclic lifetime evaluation, and the microstructure, mechanical properties were characterized to comprehensively investigate the thermal cyclic behavior of DCL TBCs compared with their counterpart of single ceramic layer TBCs.

2. Experimental

2.1. Preparation and characterization of TBCs

A commercial spherical YSZ powder (Sulzer Metco 204B-NS, −75 + 45 μm, Westbury, NY) and LZO powder (Tian-Yao Inc., −47 + 12 μm, Qing Dao, China) were used to deposit the ceramic top coat by a APS system (GP-80, JiuJiang, China). The morphology of the LZO powder and YSZ powders is shown in Fig. 1. The plasma spray parameters for the top coat are shown in Table 1. Prior to the deposition of the top-coat, a commercially available NiCoCrAlTaY powder (Amdry 997, −37 + 9 μm, Sulzer Metco, Westbury, NY) was used as the bond coat, and deposited on a nickel-based superalloy (Inconel 738, Φ25.4 mm × 3 mm) substrate. The bond coat was deposited to approximately 100 μm by a low pressure plasma spraying (LPPS) system. Table 2 shows the spraying parameters of LPPS. Before the deposition of the top coat, the as-prepared samples with bond coat were subjected to a pre-heat-treatment to forming a dense and connective Al_2O_3 TGO. The preheat-treatment process consists of two steps, namely, a pre-diffusion procedure (1080 °C +4 h, $O_2 \leq 0.01$ ppm) following by a pre-oxidation procedure (1080 °C + 4 h, $O_2 \leq 10$ ppm).

The cross-sectional microstructure and EDS analyses of the coating were characterized using a scanning electron microscope (SEM) system (TESCAN MIRA 3 LMH, Czech Republic). Before obtaining the section of samples for a metallographic examination, the samples were infiltrated with epoxy adhesive in vacuum to protect the coatings from any artifact destruction during the sample preparation. The phase composition of YSZ coatings before and after thermal cyclic test was characterized by a x-ray diffraction (XRD , PANalytical X'pert PRO, Netherlands) system. The porosity of the different regions of top coat was determined by image analysis. The cross-sectional Vickers hardness was determined by a micro-Vickers Indenter (BUEHLER MICROMET5104 , Akashi Corporation , Japan). The hardness tests were performed at a test load of 300 g and holding time of 30 s. The in-plane Young's modulus of the top coat was measured by a Knoop indentation method. The parameters and the test system were the same as for the measurement of microhardness.

Table 1
Parameters of air plasma spraying.

Parameters	YSZ	LZO
Arc current, A	650	650
Arc voltage, V	60	60
Primary plasma gas (Ar) flow, L/min	60	50
Secondary plasma gas (H_2) flow, L/min	5.5	7
Spray distance, mm	80	80

Table 2
Parameters of low-pressure plasma spraying.

Parameters	Value
Arc current, A	575
Arc voltage, V	150
Plasma gas (Ar) flow, L/min	40
Plasma gas (H_2) flow, L/min	6
Powder feeding gas (Ar) flow, L/min	1
Chamber pressure, kPa	15
Spray distance, mm	280
Torch traverse speed, mm/s	800

2.2. Thermal cyclic test for TBCs

A gas burner test setup was designed for the thermal gradient cyclic test (Xi'an Jiaotong University, China) to simulate the actual service condition of TBCs. The preset temperature of 1300 ± 30 °C/940 ± 30 °C (1300 °C at top coating surface and 940 °C at backside surface, the bond coat temperature is calculated about 1000 °C) was used to carry out the thermal gradient cyclic tests. Since the samples were heated by a propane/oxygen flame, temperature fluctuation is inevitable, but mass flowmeters with an accuracy of 0.1 SLM were

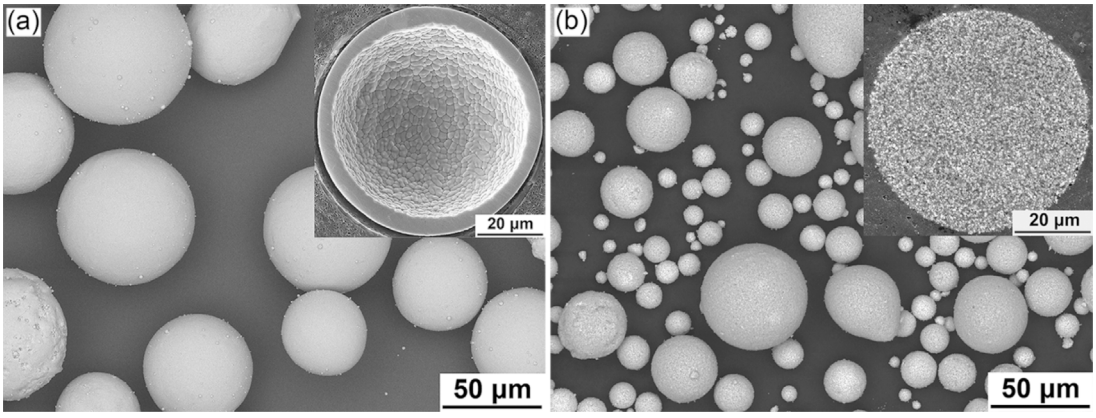

Fig. 1. Morphology of the spherical 8YSZ (a) and LZO (b) powder used for top coat. The insets show the cross section of the powder.

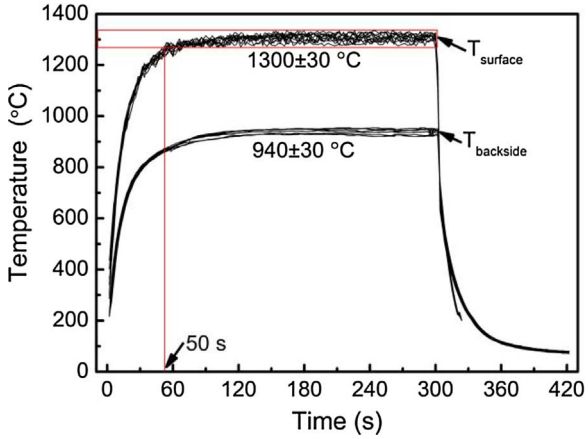

Fig. 2. Temperature changes of sample surface and backside during thermal cycle tests.

employed to ensure the stability of the flame. The temperatures of the specimen at surface and backside were monitored by non-contact infrared thermometers with wavelengths of 8–14 μm and 1.6 μm, respectively. The emissivity for YSZ and the superalloy substrate was calibrated to be 1 and 0.91 according to their wavelength, respectively. To further make the test equipment accurate prior to thermal cycle test, we carried out 100 cycles' temperature calibration test with a parallel sample before each sample test to verify the temperature fluctuation within ± 30 °C. The lifetime of TBCs was defined as the thermal cyclic lifecycles when 10% area delamination of the top coat was observed. The recorded temperatures of the sample surface and backside during thermal cycle tests are shown in Fig. 2. One thermal cycle was defined as follow: heating process, the sample surface were heated to the range of the preset temperature of 1300 ± 30 °C (in about 50 s); the holding process, the temperature of sample surface sustain at 1300 ± 30 °C (for about 250 s); the cooling process, the temperature of the sample surface drop from 1300 ± 30 °C to about room temperature (in about 120 s).

3. Results and discussion

3.1. Design of coating architecture

Thermal insulation performance is one of the fundamental functions for thermal barrier coatings. Fig. 3 shows the schematic diagram of the temperature reduction provided by the TBC. The superalloy inside surface is in contact with air for cooling, whereas the outside surface is coated with the thermal barrier coatings and in contact with hot gas, setting up a temperature gradient across the TBC. In our previous study [23], thermal resistance is introduced to evaluate the thermal insulation performance of TBCs, and it is expressed as

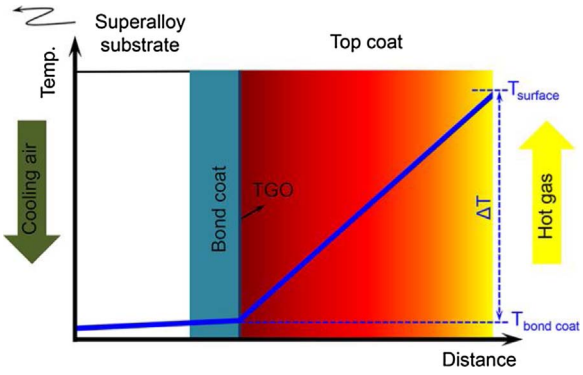

Fig. 3. Schematic diagram of the temperature reduction provided by the TBC.

$$R = \frac{\delta}{\lambda A} \quad (1)$$

Where δ is the thickness of the top coat, λ is the thermal conductivity and A is the area normal to the heat flow.

For the specific TBCs, "thermal barrier performance" is a parameter independent on the area A, hence we introduce the unit thermal resistance (UTR) as an intrinsic parameter to describe the thermal insulation performance of TBCs, it can be expressed as

$$\mathrm{UTR} = \frac{\delta}{\lambda} \quad (2)$$

For multi-layered TBCs, the TBCs are in series system, and the UTR of the multi-layers is the sum of each layer. Hence the UTR of the DCL LZO/YSZ coating can be expressed as

$$UTR = \frac{\delta_{LZO}}{\lambda_{LZO}} + \frac{\delta_{YSZ}}{\lambda_{YSZ}} \quad (3)$$

where δ_{LZO} and δ_{YSZ} is the thickness of LZO and YSZ coatings, λ_{LZO} and λ_{YSZ} is the thermal conductivity of LZO and YSZ coatings.

The thermal conductivities of plasma sprayed $La_2Zr_2O_7$[24] and YSZ [25] coatings are 0.74 W m^{-1} K^{-1} and 1.1 W m^{-1} K^{-1}, which have been measured in our previous work. Therefore, if the thermal insulation effect of 100 μm thick YSZ coating is defined as 1 unit, 67 μm thick LZO coating has exactly the same thermal insulation effect of 1 unit. According the analysis above, 5 groups of TBCs with similar thermal insulation performance were designed in this study. Fig. 4 shows the schematic diagram of the top coating architecture, namely, 500 μm YSZ (5Y), 400 μm YSZ + 67 μm LZO (4Y/1L), 300 μm YSZ + 134 μm LZO (3Y/2L), 200 μm YSZ + 201 μm LZO(2Y/3L), 100 μm YSZ + 268 μm LZO(1Y/4L). It can be found that the DCL-TBCs design is beneficial for reducing the top coating thickness.

3.2. Lifetime of TBCs

Fig. 5 shows the lifetime of different group of TBCs under thermal gradient cyclic test. The lifetime of single YSZ ceramic layer TBCs (5Y) is 91 ± 6 cycles, which is relative low due to the thicker top coat thickness of 500 μm combine with higher surface temperature of 1300 °C. When 100 μm YSZ was replaced by 67 μm LZO (namely, 4Y/1L), the lifetime was more than doubled than pure YSZ (5Y). The lifetime of DCL-TBCs decreased with the further increase of LZO replace thickness. When 200 μm YSZ was replaced, the lifetime of DCL-TBCs (3Y/2L) was still longer than 5Y. When 300 μm and 400 μm YSZ were replaced, the lifetime of DCL-TBCs (2Y/3L and 1Y/4L) decreased sharply and was much shorter than 5Y. Nevertheless, under equivalent thermal insulation performance, DCL-TBC is an effective solution to prolong the lifetime with appropriate YSZ coating thickness replaced by LZO coating.

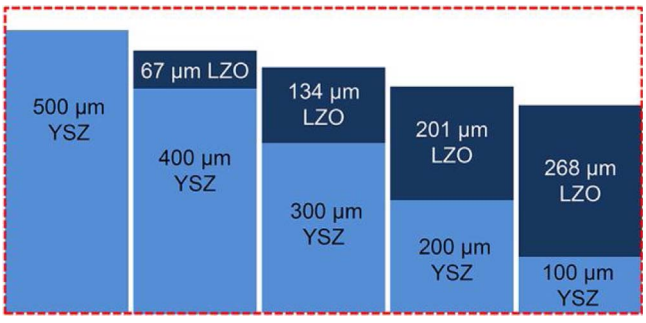

Fig. 4. Schematic diagram of the top coat architecture with the same thermal insulation effect.

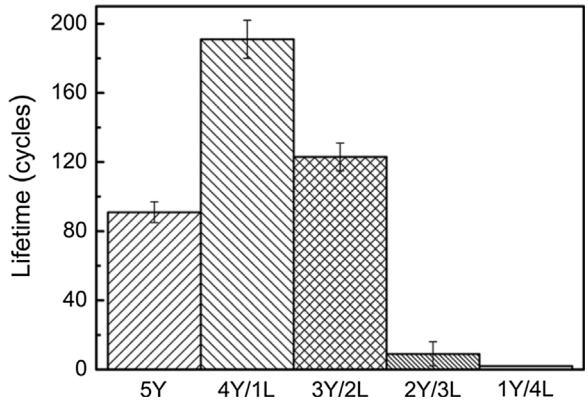

Fig. 5. Lifetime of different group of TBCs under thermal gradient cyclic test.

3.3. Failure mode

In order to clarify the failure mode of the 5 groups of TBCs, the cross sectional SEM images of as sprayed state and after failure were examined as shown in Fig. 6. For the as-sprayed TBCs, the top coats present a lamellar structure with no large cracks, and the surface shows the typical thermal sprayed features with a rough surface resulted from random stacking of splats. However, after failure, large cracks were found within top coats, and thereby the failure modes can be distinguished mainly by the location of cracks. It is found from Fig. 6(b) and (c) that, the failure mode of 5Y and 4Y/1L is the delamination within the YSZ layers. For 5Y, the distance of the failed coating surface to the bond coat is about 200 μm, which is less than the as sprayed thickness of 500 μm, and a large crack can be found as is shown in Fig. 6(b). In Fig. 6(c), a large scale crack was found within the YSZ layer proved the failure mode of 4Y/1L is the cracking inner YSZ coating. With the further increase of LZO replacing thickness, the delamination between LZO/YSZ interface happened, as shown in Fig. 6(d). Finally,

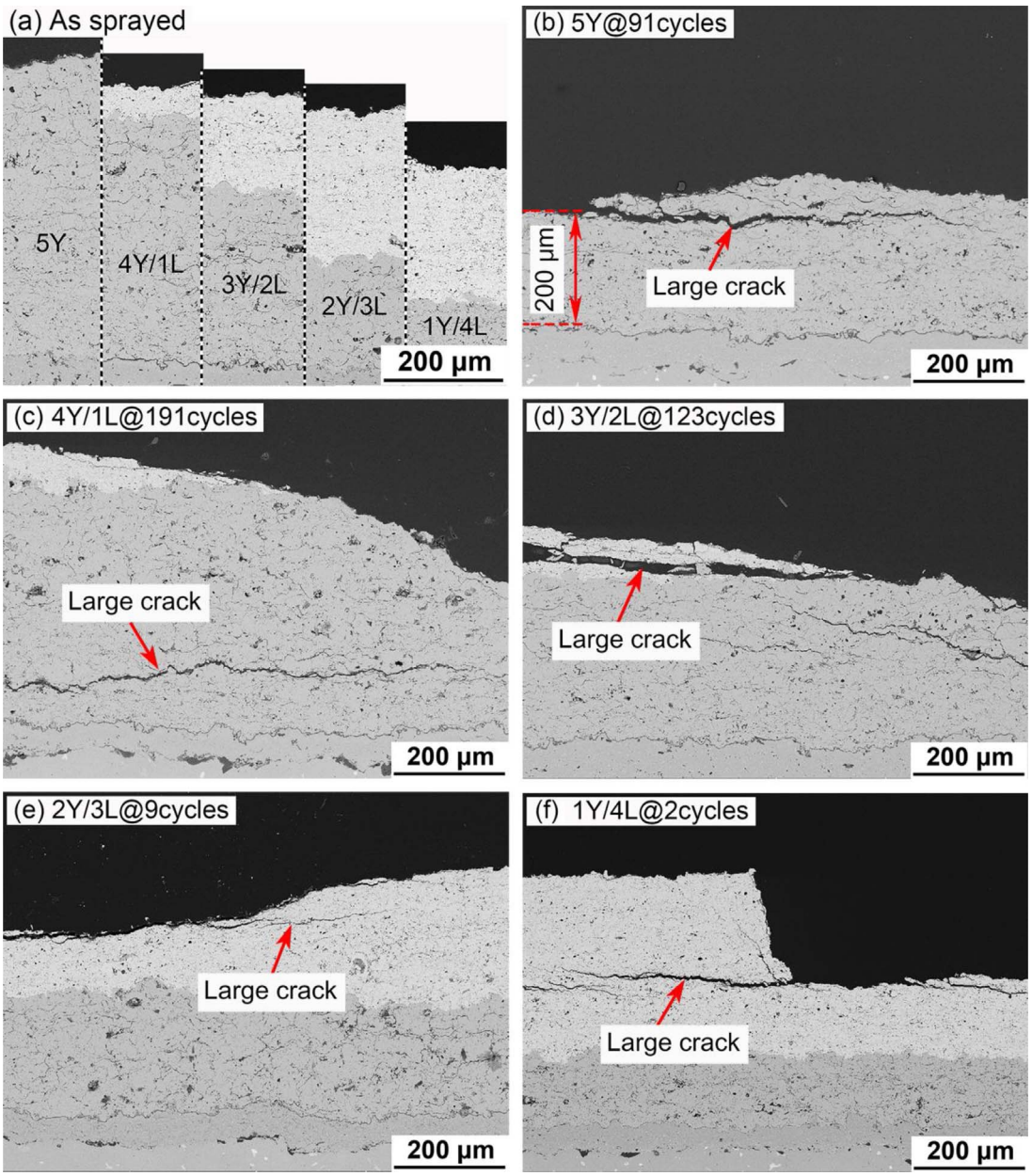

Fig. 6. The cross sectional images of different group of TBCs and their failure modes under gradient thermal cyclic test.

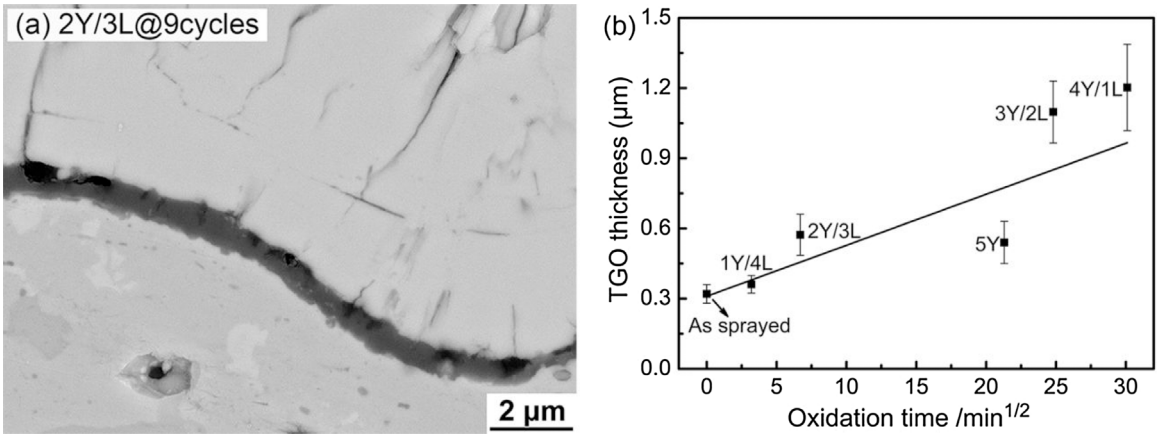

Fig. 7. The typical morphology of TGO after failure (a) and the oxidation kinetic of TGO (b).

the failure mode of 2Y/3L and 1Y/4L is a coating delamination within the LZO layer.

Therefore, it is reasonable to believe that with the increase of LZO substitutional ratio, the delamination position transferred from near top/bond coat interface to near LZO/YSZ interface and finally to the inside of the LZO coating. The delamination of the ceramic coating is essentially responsible for the failure of TBCs under thermal gradient cyclic in this study.

3.4. TGO thickness

Generally, TGO growth is considered as one of the important factors leading to the failure of TBCs[26,27]. Thus, the TGO growth behavior in the present TBC samples was examined. It was found from Fig. 6(b)–(f) that no obvious cracks were observed close to the TGO, suggesting that the TGO may not be responsible for the failure of TBCs in this study. As a further step, TGO thickness was determined by the cross-sectional SEM micrographs before and after thermal cyclic test, and each value was the mean thickness of 10 different regions of TGO.

Fig. 7(a) shows the morphology of TGO for the failure samples of 2Y/3L after about 123 cycles. It can be found that the TGO is uniform and dense. TGO thickness in the as-sprayed TBCs was 0.32 ± 0.04 μm, resulting from the pre-treatment mentioned in Section 2.1. After thermal cyclic test to failure, the TGO slightly thickened with respect to that in the as-sprayed TBC. The thicknesses of TGO were 0.54 ± 0.09 μm, 1.20 ± 0.18 μm, 1.10 ± 0.13 μm, 0.57 ± 0.08 μm and 0.36 ± 0.04 μm for the failure samples of 5Y, 4Y/1L, 3Y/2L, 2Y/3L and 1Y/4L, respectively. The square root of equivalent holding time was calculated and plotted with the TGO thickness. The scattered points were well fitted with a straight line, revealing that the TGO thickness presented a good parabolic relationship with the oxidation duration.

Although the TGO thicknesses after thermal cyclic test were thicker than that in the as-prepared samples, they were significantly smaller than the reported critical value to induce a complete delamination of top coat, i.e., 5–6 μm [27]. It is evidently proved that the slightly thickening of TGO is not the dominant factor responsible for the failure of TBCs in this study.

3.5. Phase composition of the top coat

Given the fact that phase transformation might be a reason to induce the spallation of YSZ top coat, the phase composition of the top coat after TBC failure was examined, as shown in Fig. 8. It can be found from Fig. 8(a) that the phase compositions of the YSZ coatings before and after thermal cyclic test were mainly non-transformable t'-phase. Little peaks of monoclinic and cubic phase were found in the as sprayed state, and they both showed no obvious increase when compared with the coatings after thermal cyclic tests. That means no distinct phase transformation caused by the thermal cyclic test, therefore, it is convinced that phase transformation is not responsible for the failure of pure YSZ (5Y) coatings.

It is seen from Fig. 8(b) that, a little peak of ZrO_2 was found after thermal cyclic tests, they are bigger than those in the as sprayed state. However, when compared with the main peaks of pyrochlore LZO, these peaks are still very small. And we believe the growth of ZrO_2 peaks were caused by different scan regions during XRD test, it is also supported by the EDS results in Fig. 9. It is seen from Fig. 9 that, the elements of plasma sprayed LZO coatings showed an uneven distribution. Very narrow stripped regions with La/Zr ratio less than the pyrochlore structured LZO of 0.87–1.15 were detected before and after thermal cyclic test. This is caused by the loss La_2O_3 during plasma spray process which can lead to an uneven stoichiometry within the LZO [18,19], especially for high torch input power[28]. Although the uneven stoichiometry of LZO might be a reason for the failure of LZO coatings, the XRD results showed that the main phase is still pyrochlore structured LZO after thermal cyclic test, and we do believe there must be some other important reasons responsible for the failure of LZO/YSZ TBCs in this study.

3.6. Differential sintering of the top coat

During service, high temperature exposure with extended periods often leads to inevitable sintering of the ceramic top coat [29]. As described above, sintering ceramic coatings are accompanied by the reduction of coating porosity[30] and strain tolerance, the increase of elastic modulus and thermal conductivity. In this study, TBCs were exposed to a gradient temperature condition. Dependent on the regions along through-thickness direction, high temperature exposure induced distinct changes in properties of the top coat. However, the overall properties, such as strain tolerance and thermal conductivity can not embody the difference across the thickness. Therefore, the localized densification phenomenon through SEM images was examined. Fig. 10 shows the high-magnification images of different regions after failure (4Y/1L @ 191 cycles). In order to reveal the inhomogeneous sintering behavior across the thickness of the ceramic top coat, the unpeeling cross-sections of the ceramic coatings were divided into 5 regions according to their distance away from the TGO/BC interface, shown in Fig. 10(a). It is found in Fig. 10(b), that in the near coating surface of region 5, random arranged spherical pores are distributed all over this region. A step near to bond coat of the region 4, as shown in Fig. 10(c), spherical pores are obvious being smaller than that of region 5, and the spherical pores present a regular distribution with the sign of lamellar structure. For the middle locations of region 3, shown in Fig. 10(c), the large scale of lamellar structure was reserved, and the spherical pores

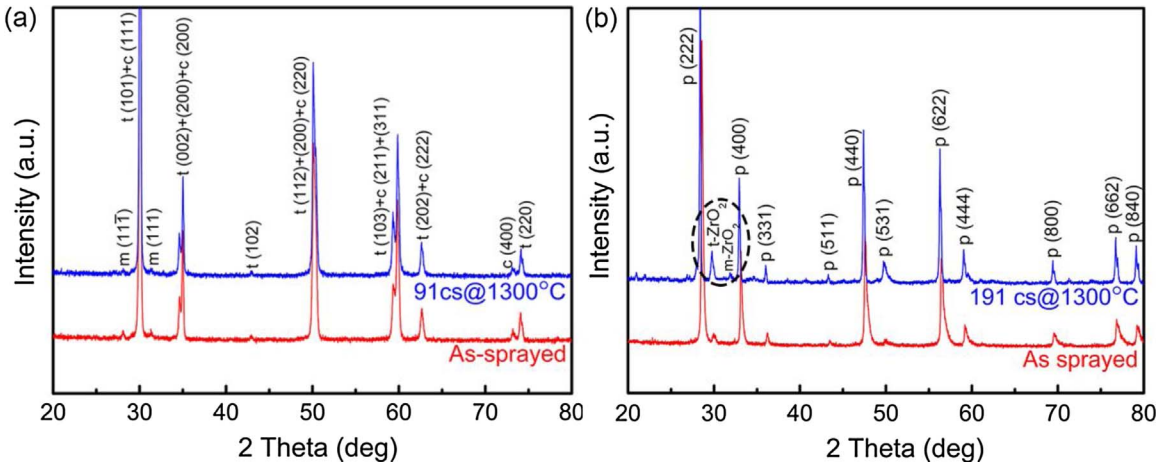

Fig. 8. XRD patterns of the top-coat before and after thermal cyclic tests: (a) YSZ and (b) LZO.

were rarely found. For the inner regions of 2 and 1, the lamellar structure was nearly completely reserved because of relatively low temperature.

In order to further confirm the differential distribution of the property of top coats across coating thickness, the porosity of different regions was examined, as shown in Fig. 11. Compared with the as sprayed state, the porosity of top coat after failure showed more or less decrease because of high temperature exposure. The larger thermal cycles, the more of the porosity decreased. For a certain sample in YSZ layers, the porosity shows a differential distribution, (e.g. 5Y, region 1–4 of 4Y/1L, region 1–3 of 3Y/2L and region 1–2 of 2Y/3L). The porosity of LZO layers shows not that great difference, for the region 5, the porosity of 5Y, 4Y/1L and 3Y/2L decreased about 40%-45% compared with the as sprayed state, and 2Y/3L and 1Y/4L also decreased about 12%-22%. However, region 1 shows nearly no decrease in porosity because of relatively low temperature. It is convinced that the differential sintering happened during gradient thermal cyclic test.

The elastic modulus is one of most important parameters for the sintering evaluation[32], and the value depends on the exposure time and temperature. Fig. 12 shows the elastic modulus of different regions before and after thermal cyclic test. The as-sprayed YSZ and LZO top coatings present homogeneous microstructure and mechanical properties, and the elastic modulus at different regions are the same, i.e. 65 GPa and 64 GPa YSZ and LZO top coatings, respectively. However, after failure, the elastic modulus presents a differential distribution. The elastic modulus of YSZ and LZO could reach values as high as 95 GPa and 142 GPa, respectively. The elastic increase of LZO is well consistent with the date reported in the papers on the high temperature exposure of plasma sprayed LZO coatings, when the holding time was converted to equivalent duration[27]. It has been reported that, higher temperature accelerates the sintering of coatings[7,31]. For example, in T. W. Clyne's study[32], when the sintering temperature increased from 1000 °C to 1300 °C, the elastic modulus of the plasma sprayed TBC top coatings increased 3 ~ 4 times. In our present study, the surface temperature of the thermal cyclic tests was set to be 1300 ± 30 °C, which was high enough to cause the fast sintering for top coatings. It is also reported that, the elastic modulus increased rather rapidly at the very beginning according to the two-stage sintering mechanism for TBC[33,34]. In our previous study[35], we demonstrated that, for the sintering of a specific top coating, a certain degree of sintering can be achieved by higher temperature of shorter time or a relative lower temperature of a longer time. Therefore, it is convinced that the elastic modulus increased faster at the regions closer to the top coat surface due to the temperature gradient across the coating thickness and slower close to the bond coat because of relative lower temperature.

3.7. Failure analysis

After thermal cyclic tests at different conditions, at least three aspects can be clearly distinguished. To begin with, the maximum thickness of TGO is about 1.2 μm, being far less than the critical value of 5–6 μm to induce a completely delamination of the top coat. Secondly, the YSZ top coat showed no obvious phase transformation and the thermal cyclic test does not increase the decomposition of LZO during high temperature thermal cyclic test. Thirdly, dependent with the regions along through-thickness direction, high temperature

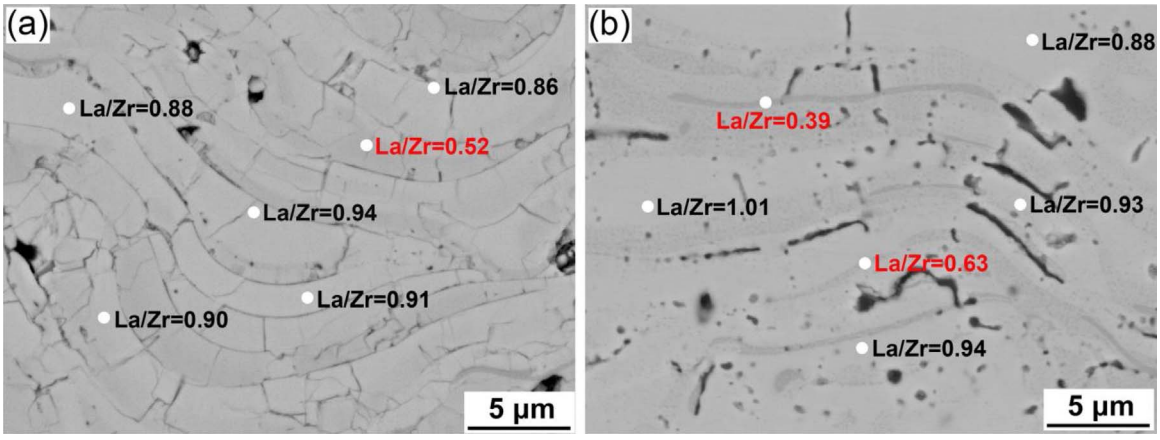

Fig. 9. Quantitative EDS elemental analyses of the LZO coating for as sprayed (a) and after thermal cycle to failure (b) of 4Y/1L. The indicated La/Zr ratios are atomic ratios.

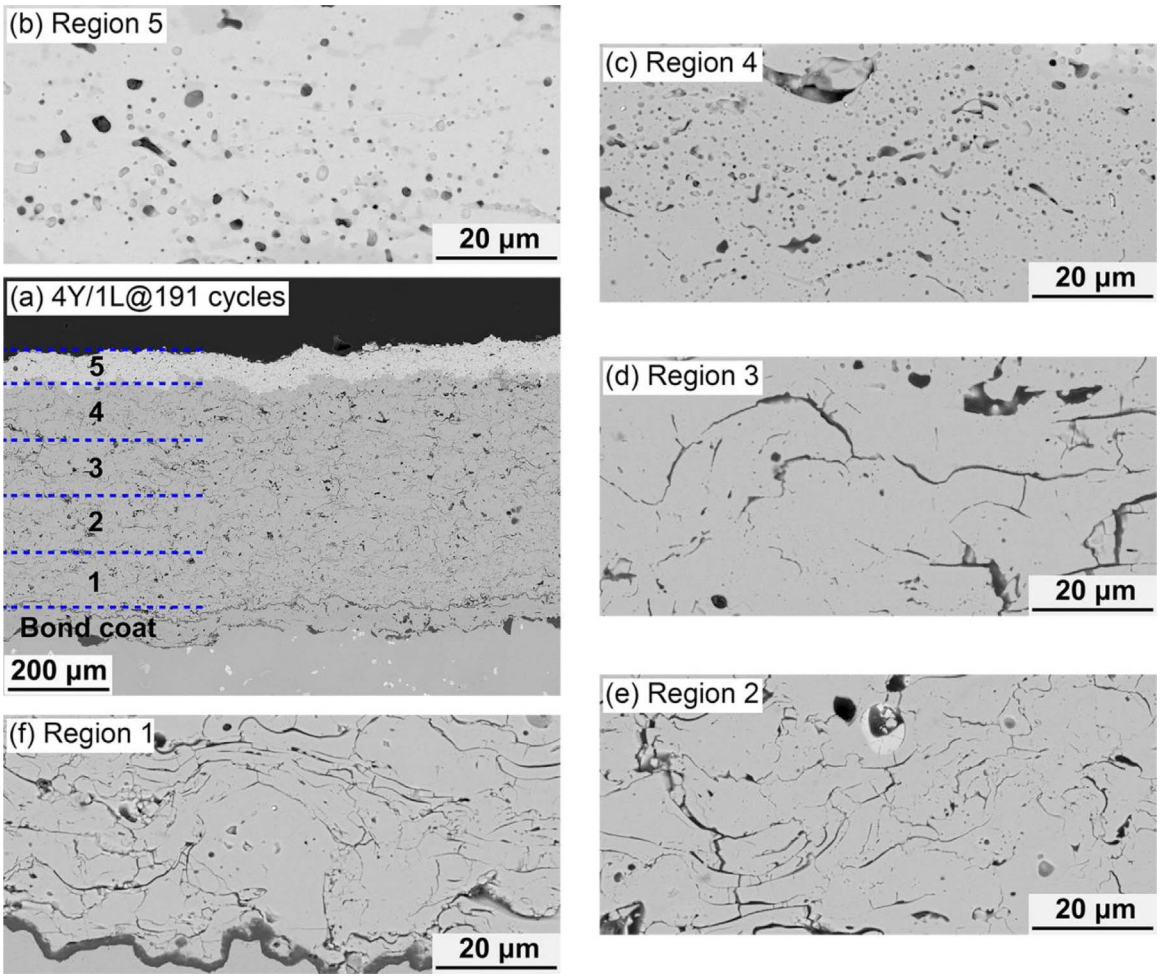

Fig. 10. High-magnification images of different regions after failure (4Y/1L @ 191 cycles).

exposure induced distinct changes in properties of the top coat. The significantly stiffened top coat dominates the delamination of TBCs.

It can be concluded that, the failure of TBCs is mainly dominated by the crack propagated within the top coats. The crack propagation occurs when the strain energy release rate is larger than the critical interfacial crack energy or fracture toughness. The strain energy release rate, G_h, can be obtained as follow:

$$G_h = \begin{cases} \int_0^{h_1} \frac{E_Y \varepsilon^2}{2(1-\nu)} dx & \text{for 5Y} \\ \int_0^{h_1} \frac{E_Y \varepsilon^2}{2(1-\nu)} dx + \int_{h1}^{h2} \frac{E_L \varepsilon^2}{2(1-\nu)} dx & \text{for 4Y} \\ \int_0^{h_2} \frac{E_Y \varepsilon^2}{2(1-\nu)} dx & \text{for 3Y/2L, 2Y/3L and 1Y/4L} \end{cases} \quad (4)$$

where h is the distance from the crack tip to top coating surface, h_1 and h_2 is the distance from the crack tip to the YSZ and LZO surface, respectively. E_Y and E_L is the local elastic modulus of YSZ and LZO at the crack tip, ε is the strain, ν is the Poisson's ratio.

As the analysis above, G_h increases with the increase of h, the coat

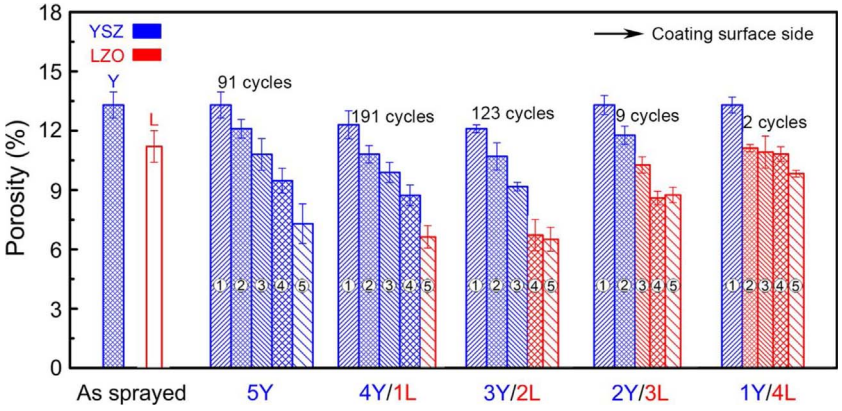

Fig. 11. Porosity of different regions before and after thermal cyclic test.

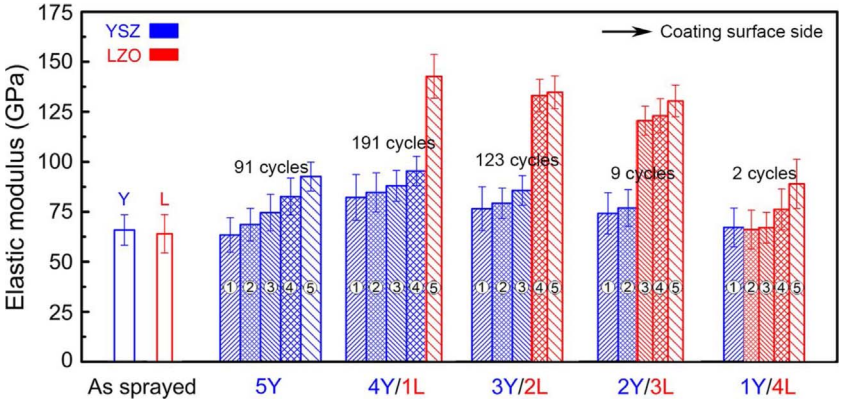

Fig. 12. Elastic modulus of different regions before and after thermal cyclic test.

failure happened with certain thickness. Furthermore, the sintering induced gradient distribution of mechanical properties makes the G_h increase more significantly. On the other hand, sintering caused the densification of ceramic coating will increase the cracking resistance. Therefore, whether the crack propagates mainly depends on the competition between the cracking driving force and the cracking resistance i.e., strain energy release rate and localized fracture toughness of the top coat. For 4Y/1L, the thickness of LZO is just 67 μm, the driving force in LZO layer is not enough to cause the cracking of LZO, combining with that the cracking resistance increased because of the long term high temperature exposure. The failure happens within the under YSZ layer. With the increase of LZO, the driving force increased and the failure located at LZO/YSZ interface. For 2Y/3L and 1Y/4L, since the thickness of LZO is 3–4 times of the 4Y/1L, G_h increased remarkably. However, the intrinsic property of LZO exhibits a low CTE and/or a poor fracture toughness. On the other hand, the contribution of sintering to the cracking resistance is limited (at most 9 cycles). Consequently, with the increase of LZO substitutional ratio, the delamination position transferred from near top/bond coating interface to near LZO/YSZ interface and finally to the inside of LZO coating.

4. Conclusions

Double ceramic layer TBCs were designed and subjected to thermal gradient tests based on the concept of equivalent thermal insulation performance proposed in this study, with the aim to reveal the failure behavior of DCL-TBCs. YSZ/LZO TBCs are examined as an example of typical DCL-TBCs. The following conclusions could be obtained from this work:

(1) The lifetime of YSZ and double layer coatings is at least an order of magnitude lower than results found under similar loading conditions in literature, which may be caused by the thick top coat thickness of 500 μm combined with higher temperature of 1300 °C.
(2) Equivalent thermal insulation concept is introduced for the design of double ceramic coatings with different component layer ratio. TBCs with equivalent insulation performance of 500 μm YSZ coatings were designed. With the increase if LZO proportion, the total thickness of DCL TBCs decreased.
(3) The lifetime of conventional 5Y is about 91cycles under the surface/backside temperature of 1300/940 °C gradient thermal cyclic test, while the lifetime of 4Y/1L DCL-TBCs showed up to 2 times higher than that of 5Y, proving that the DCL-TBCs is an effective technique for the application of TBCs in higher temperature with longer lifetime.
(4) The maximum thickness of TGO in failed TBC samples was 1.2 μm, being far less than the critical value causing the failure of TBCs through complete delamination of the top coat. The thermal cyclic test does not cause the YSZ phase transformation or the decomposition of LZO during high temperature thermal cyclic test. Therefore, the above aspects are not the essential reasons responsible for the failure of TBC in the present study.
(5) The lamellar cracking within top coating was the essential failure reason for both 5Y and DCL-TBCs. With the increase of LZO substitutional ratio, the delamination position transferred from near top/bond coating interface to near LZO/YSZ interface and finally to the inside of LZO coating.
(6) The porosity and elastic modulus present a differential distribution across the thickness of top coat due to the temperature gradient in thermal cyclic test, which means the differential sintering of top coat. The competition between the cracking driving force and the cracking resistance determine the failure mode of TBCs.

Acknowledgments

The present project is supported by National Basic Research Program (Grant No. 2013CB035701), the National Science Foundation of China (Grant No. 51671159), the Fundamental Research Funds for the Central Universities, and the National Program for Support of Top-notch Young Professionals.

References

[1] N.P. Padture, M. Gell, E.H. Jordan, Thermal barrier coatings for gas-turbine engine applications, Science 296 (5566) (2002) 280–284.
[2] J. Li, H. Liao, X. Wang, C. Coddet, Fractal Perimeters of Polishing-Induced Pull-Outs Present on Polished Cross Sections of Plasma-Sprayed Yttria-Stabilized Zirconia Coatings, J Am. Ceram. Soc. 86 (11) (2003) 1906–1910.
[3] X.Q. Cao, R. Vassen, D. Stoever, Ceramic materials for thermal barrier coatings, J. Eur. Ceram. Soc. 24 (1) (2004) 1–10.
[4] D.R. Clarke, M. Oechsner, N.P. Padture, Thermal-barrier coatings for more efficient gas-turbine engines, MRS Bull. 37 (10) (2012) 891–898.
[5] G.W. Goward, Progress in coatings for gas turbine airfoils, Surf. Coat. Technol. 108 (1-3) (1998) 73–79.
[6] D.R. Clarke, S.R. Phillpot, Thermal barrier coating materials, Mater. Today. 8 (6) (2005) 22–29.
[7] R.W. Trice, Y.J. Su, J.R. Mawdsley, K.T. Faber, A.R. De Arellano-Lopez, H. Wang, W.D. Porter, Effect of heat treatment on phase stability, microstructure, and thermal conductivity of plasma-sprayed YSZ, J. Mater. Sci. 37 (11) (2002) 2359–2365.
[8] J. Ilavsky, J.K. Stalick, Phase composition and its changes during annealing of plasma-Sprayed YSZ, Surf. Coat. Technol. 127 (2) (2000) 120–129.
[9] T. Vogt, B.A. Hunter, J. Thornton, Structural evolution of thermal-Sprayed yttria-Stabilized ZrO_2 thermal barrier coatings with Annealing-A neutron diffraction study, J. Am. Ceram. Soc. 84 (3) (2001) 678–680.
[10] S. Paul, A. Cipitria, I.O. Golosnoy, L. Xie, M.R. Dorfman, T.W. Clyne, Effects of impurity content on the sintering characteristics of plasma-sprayed zirconia, J. Therm. Spray Technol. 16 (5) (2007) 798–803.
[11] L. Lorenzoni, S. Ahmaniemi, Studies of the sintering kinetics of thick thermal barrier coatings by thermal diffusivity measurements, J. Eur. Ceram. Soc. 25 (4) (2005) 393–400.
[12] K. Fritscher, F. Sziics, U. Schulz, B. Saruhan, M. Peters, W.A. Kaysser, Impact of thermal exposure of EB-PVD TBCs on young's modulus and sintering, CESP 23 (4) (2002) 341–352.
[13] H. Dai, X. Zhong, J. Li, Y. Zhang, M. Jian, X. Cao, Thermal stability of double-ceramic-layer thermal barrier coatings with various coating thickness, Mater. Sci. Eng. A. 433 (1) (2006) 1–7.

[14] Z. Xu, L. He, R. Mu, X. Zhong, Y. Zhang, J. Zhang, X. Cao, Double-ceramic-layer thermal barrier coatings of $La_2Zr_2O_7$/YSZ deposited by electron beam-physical vapor deposition, J. Alloys. Compd. 473 (1-2) (2009) 509–515.
[15] R. Vaßen, F. Traeger, D. Stöver, New thermal barrier coatings based on Pyrochlore/YSZ double-layer systems, Int. J. Appl. Ceram. Tec. 1 (4) (2004) 351–361.
[16] H. Chen, Y. Gao, S. Tao, Y. Liu, H. Luo, Thermophysical properties of lanthanum zirconate coating prepared by plasma spraying and the influence of post-annealing, J. Alloys. Compd. 486 (1–2) (2009) 391–399.
[17] A.K. Rai, M.P. Schmitt, R.S. Bhattacharya, D.M. Zhu, D.E. Wolfe, Thermal conductivity and stability of multilayered thermal barrier coatings under high temperature annealing conditions, J. Eur. Ceram. Soc. 35 (5) (2014) 1605–1612.
[18] X.Q. Cao, R. Vassen, W. Jungen, S. Schwartz, F. Tietz, D. Stover, Thermal stability of lanthanum zirconate plasma-sprayed coating, J. Am. Ceram. Soc. 84 (9) (2001) 2086–2090.
[19] H. Chen, Y. Liu, Y. Gao, S. Tao, H. Luo, Design preparation, and characterization of graded YSZ/$La_2Zr_2O_7$Thermal barrier coatings, J. Am. Ceram. Soc. 93 (6) (2010) 1732–1740.
[20] K. Kokini, J. DeJonge, S. Rangaraj, B. Beardsley, Thermal shock of functionally graded thermal barrier coatings with similar thermal resistance, Surf. Coat. Technol. 154 (2–3) (2002) 223–231.
[21] L. Wang, Y. Wang, X.G. Sun, J.Q. He, Z.Y. Pan, C.H. Wang, Thermal shock behavior of 8YSZ and double-ceramic-layer $La_2Zr_2O_7$/8YSZ thermal barrier coatings fabricated by atmospheric plasma spraying, Ceram. Int. 38 (5) (2012) 3595–3606.
[22] R. Vassen, X. Cao, F. Tietz, D. Basu, D. Stöver, Zirconates as new materials for thermal barrier coatings, J. Am. Ceram. Soc. 83 (8) (2000) 2023–2028.
[23] H. Xie, Y.C. Xie, G.J. Yang, C.X. Li, C.J. Li, Modeling thermal conductivity of thermally sprayed coatings with intrasplat cracks, J. Therm. Spray Technol. 22 (8) (2013) 1328–1336.
[24] T. Liu, X. Chen, G.J. Yang, C.J. Li, Properties evolution of plasma-sprayed $La_2Zr_2O_7$ coating induced by pore structure evolution during thermal exposure, Ceram. Int. 42 (14) (2016) 15485–15492.
[25] H. Dong, G.J. Yang, H.N. Cai, C.X. Li, C.J. Li, Propagation feature of cracks in plasma-sprayed YSZ coatings under gradient thermal cycling, Ceram. Int. 41 (3) (2015) 3481–3489.
[26] A. Rabiei, A.G. Evans, Failure mechanisms associated with the thermally grown oxide in plasma-sprayed thermal barrier coatings, Acta Mater. 48 (15) (2000) 3963–3976.
[27] H. Dong, G.J. Yang, C.X. Li, X.T. Luo, C.J. Li, Effect of TGO thickness on thermal cyclic lifetime and failure mode of plasma-sprayed TBC s, J. Am. Ceram. Soc. 97 (4) (2014) 1226–1232.
[28] G. Mauer, D. Sebold, R. Vassen, D. Stöver, Improving atmospheric plasma spraying of zirconate thermal barrier coatings based on particle diagnostics, J. Therm. Spray Technol. 21 (3) (2012) 363–371.
[29] W. Chi, S. Sampath, H. Wang, Microstructure-Thermal conductivity relationships for plasma-Sprayed yttria-Stabilized zirconia coatings, J. Am. Ceram. Soc. 91 (8) (2008) 2636–2645.
[30] H.B. Guo, S. Kuroda, H. Murakami, Microstructures and properties of plasma-Sprayed segmented thermal barrier coatings, J. Am. Ceram. Soc. 89 (4) (2006) 1432–1439.
[31] D.M. Zhu, R.A. Miller, Thermal conductivity and elastic modulus evolution of thermal barrier coatings under high heat flux conditions, J. Therm. Spray Technol. 9 (2) (2000) 175–180.
[32] J.A. Thompson, T.W. Clyne, The effect of heat treatment on the stiffness of zirconia top coats in plasma-sprayed TBCs, Acta Mater. 49 (9) (2001) 1565–1575.
[33] G.R. Li, H. Xie, G.J. Yang, G. Liu, C.X. Li, C.J. Li, A comprehensive sintering mechanism for TBCs-Part I: An overall evolution with two-stage kinetics, J. Am. Ceram. Soc. 100 (5) (2017) 2176–2189.
[34] G.R. Li, H. Xie, G.J. Yang, G. Liu, C.X. Li, C.J. Li, A comprehensive sintering mechanism for TBCs-Part II: Multiscale multipoint interconnection enhanced initial kinetics, J. Am. Ceram. Soc. 100 (9) (2017) 4240–4251.
[35] B. Cheng, Y.M. Zhang, N. Yang, M. Zhang, G.J. L.Chen, et al., Sintering-induced delamination of thermal barrier coatings by gradient thermal cyclic test, J. Am. Ceram. Soc. 100 (5) (2017) 1820–1830.